 doi:10.20944/preprints202205.0132.v1

Article

The effect of entrapment within sol-gel magnetite on Carbonic anhydrase

Vladimir Ivanovski[1], Olga Shapovalova[2], Andrey S. Drozdov[3]*

[1] Ss. Cyril and Methodius University in Skopje, Faculty of Natural Sciences and Mathematics, Institute of Chemistry, Arhimedova 5, 1000 Skopje, Macedonia; vladimir.ivanovski@yahoo.com
[2] ITMO University, SCAMT Institute, Lomonosova st. 9, 191002 Saint Petersburg, Russia; shapovalova@scamt-itmo.ru
[3] Moscow Institute of Physics and Technology, Institutsky ave. 9, Dolgoprudny, Moscow Region, Russia; drozdov.science@gmail.com
* Correspondence: vladimir.ivanovski@yahoo.com (V.I.); drozdov.science@gmail.com (A.D.)

Abstract: Enzymatically active nanocomposites are a perspective class of bioactive materials that finds their application in numerous fields of science and technology ranging from biosensors and therapeutic agents to industrial catalysts. Key properties of such systems are their stability and activity under various conditions, the problems that are addressed in any research devoted to this class of materials. omprehension the principles that affect these properties play the most important role in the development of the field, especially when it takes to a new class of bioactive systems. Recently, a new class of enzymatically doped magnetite-based sol-gel systems emerged and paved the way for a variety of potent bioactive magnetic materials with improved thermal stability. Such systems already showed themself as perspective industrial and therapeutic agents, but are still under intense investigation and many aspects are still unclear. Here we made a first attempt to describe the interaction of biomolecules with magnetite-based sol-gel materials and to investigate facets of protein structure rearrangements occurring within the pores of magnetite sol-gel matrix using dedicate Fourier-transform infrared spectroscopy.

Keywords: magnetite; sol-gel; carbonic anhydrase; protein secondary structure; entrapment, infrared spectroscopy

1. Introduction

Enzymatic nanocomposites and hybrid materials are emerging classes of bioactive materials which attract a vast amount of attention due to the potential contained in such systems for a variety of applications. Enzymatic composites are intensively studied for the purposes of industrial applications, analytics, smart materials, and next-level nanotherapeutics[1–5]. Such composites may be synthesized in a variety of ways depending on the proposed application scenario, but among them, special attention can be paid to sol-gel composites. Sol-gel materials have shown themselves as excellent carriers of small biomolecules, proteins, and even whole cells by the so-called entrapment strategy[6–8]. This approach is based on the process of *in-situ* gelation of the corresponding sols in presence of corresponding dopants, which become physically trapped within forming gel structures. The high porosity of the resulting composites ensures steady mass transfer inside such systems allowing trapped species to maintain their catalytic activities and at the same time preventing them from leaching into surrounding media due to sterical reasons[9,10]. Moreover, it was reported that incorporation of biopolymers into the porous structure of the final material may enhance their stability towards numerous destructive factors, such as high temperature or oxidizing agents[11,12]. As the result, many bioactive systems were described, such as highly stable biosensors, industrially important biocatalysts, or even cell-based implants[13–15]. The imposed stability of the immobilized agents is implemented by several factors. First of all, encapsulated biomolecules are protected from biodegradation by enzymes or microorganisms. Second, it should be taken into consideration that the gel microenvironment can be highly hydrated due to water molecules

check for updates

Citation: Ivanovsi, V.; Shapovalova, O; Drozdov, A. Title. *Preprints* **2022**, *1*, 0. https://doi.org/

Received:
Accepted:
Published:

Preprints (www.preprints.org) | NOT PEER-REVIEWED | Posted: 10 May 2022 doi:10.20944/preprints202205.0132.v1

tightly associated with the material of the porous matrix[16]. And lastly, the structure of biomolecules can be stabilized by the form of the pores themselves, densely surrounding the dopant. These effects can be even further improved by the addition of osmolytes or hydrophilic agents, resulting in highly stable systems which can be stored on a shelf at room temperature for long periods without degradation, giving rise to a variety of potential application scenarios of such systems[17]. The majority of sol-gel systems are based on silica as it was the first and best-studied sol-gel material suitable for entrapment, while in recent years several more systems were invented[18–20]. Among them, a special place should be given to magnetic sol-gel systems based on iron oxides due to the unique magnetic properties of such materials[21,22]. Magnetic sol-gel systems are interesting not only due to their ability to be localized or extracted with constant magnetic fields but also due to their sensitivity to alternating radio-frequency fields which can be used for localized heating of those materials and even for control over their catalytic activity, allowing to couple physical stimuli and biochemical reactions[23]. Been one of the most recent enzymatically-active sol-gel systems magnetite-based hybrid materials still under intense investigation and still lacks proper description and understanding of the observed phenomenons. Here we, to the best of our knowledge, make the first attempt to describe and explain previously observed increased stability of enzymes entrapped within magnetite sol-gel matrix taking carbonic anhydrase as the model. By careful analysis of the hybrid material with Fourier-transform infrared spectroscopy (FTIR) and circumscribing the alternation in the entrapped enzyme's secondary structure, we are giving our vision on the processes taking place inside pores of the magnetic bioceramic and shedding light on the fate of the protein inside the opaque matrix.

2. Results

Ferria hydrosol used in this study was synthesized via an ultrasonically-assisted co-precipitation synthetic strategy that gives a stable hydrosol of magnetite NPs in water at a neutral pH level. The produced magnetite nanoparticles had a mean diameter of 10 nm according to XRD, SEM, and TEM analysis with a truncated tetrahedron morphology, typical for co-precipitation synthetic procedures (Fig. 1a-c), while the application of non-stochiometric ratio of iron (II) and (III) ions led to the enrichment of the NPs surface with Fe(II)-OH groups that shifted their isoelectric point to higher pH level of 8.2-8.4. As the result, the resulted system had a significantly higher zeta potential of +31 mV, ensuring their colloidal stability at neutral or slightly basic pH levels and in the presence of low salt concentrations. Moreover, the pristineness of their surface of any modifiers, such as surfactants or citrate ions, allowed such NPs to undergo sol-gel transition after partial solvent removal, resulting in stable mesoporous sol-gel matrices (Ferria) via the formation of Fe-O-Fe inter-particle bonds[24]. This fact allowed to use of such matrices for the entrapment of proteins or enzymes under mild conditions.

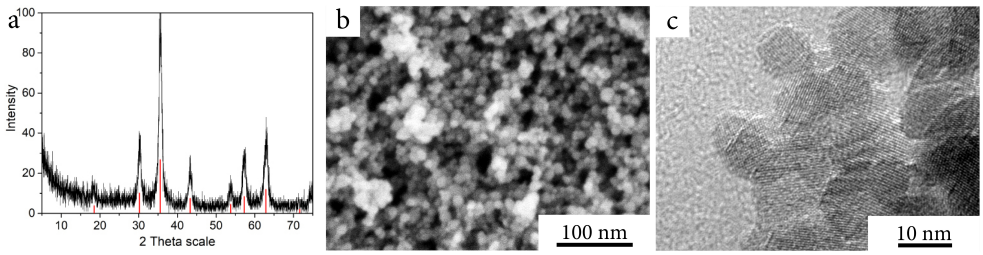

Figure 1. Magnetite nanoparticles: (**a**) XRD pattern of the synthesized material. (**b**) SEM image of the material. (**c**) TEM image of the material.

The porous structure of sol-gel Ferria ensured mass transfer within the material and allowed entrapped CAB to retain its catalytic activity at the level of 8% of its initial values at 20 ∘C. At the same time, the immobilized enzyme showed significantly higher thermal stability and preserved its enzymatic activity even at 90 ∘C, while the free enzyme totally

Preprints (www.preprints.org) | NOT PEER-REVIEWED | Posted: 10 May 2022 doi:10.20944/preprints202205.0132.v1

denatured at 70 ∘C (See Table 1 and Fig. 2a). It can be seen, that T_{opt} for hybrid material is shifted approximately 20 ∘C higher compared to free enzyme due to stabilizing effect of 3D matrix and elevated mass transfer processes in the porous material.

Table 1. pNPA conversion rate as a function of temperature for CAB and CAB@Ferria.

Temperature, ∘C	CAB, μM/min	CAB@Ferria, μM/min
20	3.30	0.27
30	4.18	0.56
40	4.80	0.87
50	4.66	1.30
60	2.80	1.82
65	0.80	1.79
70	0	1.62
80	0	1.30
90	0	0.79

Enhanced thermal stability of immobilized CAB can be seen from DCS curves of the free enzyme and CAB@Ferria (Fig. 2B). The peak corresponding to maximal heat consumption corresponding to the biomolecule's structure rearrangement and its denaturation is shifted for 30 ∘C to a higher temperature, proving enhanced stability of the immobilized enzyme.

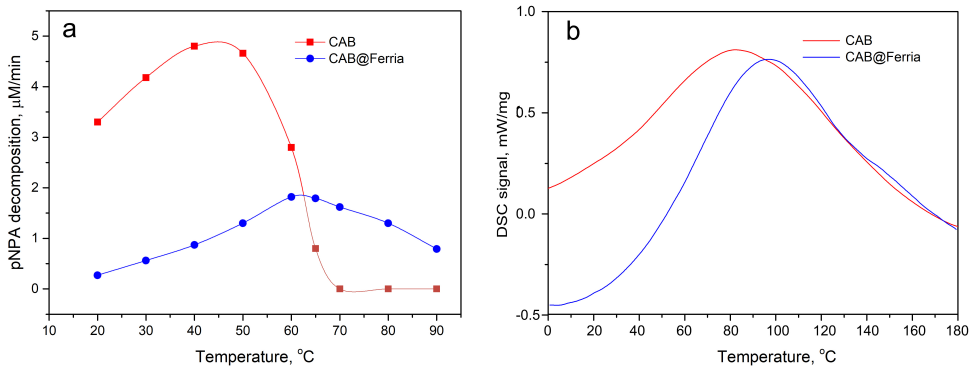

Figure 2. Thermal behaviour of free CAB and CAB@Ferria: (**a**) Catalytic activity of free CAB and CAB@Ferria as a function of temperature. (**b**) DCS curves of free CAB and CAB@Ferria.

More detailed investigations of the occurring rearrangements were done using infrared spectroscopy. Protein structure dependence on temperature has been investigated a lot. The investigation of ribonuclease-A and myoglobin structure as a function of temperature[25] shows that helical structures are more affected than β-sheet. That this is the case was also presented by the formation of a molten globular state in β-lactoglobulin[26], where at temperatures of 70 °C almost all β-helix and one-fifth of the β-sheet was lost, compared to the native structure. This kind of molten globular state was introduced in the work on Bovine Carbonic Anhydrase (CAB)[27], where the changes in the structure of the protein with the temperature at pH 2.6 were discussed. It appears that raising the temperature to 67 ∘C, one-third of the β-sheet was lost in a non-cooperative way, while the rest, until 87 °C in a cooperative manner. The percentage of β-sheet in CAB as reported in[27] is ca. 40%. The more precise measurements using FTIR, X-Ray, and Circular Dichroism[28], report this percentage to be 49%, while β-helix 13%. In all the above references, the Amide I band was investigated in order to establish the percentage of secondary structures, but also to investigate its intensity and frequency change with temperature[25–27]. As proposed in ref.[28] and further supported in [29], the Amide I band of CAB can be deconvoluted in 8 bands: 1625, 1636 and 1678 cm^{-1} β-structures, 1653 cm^{-1} Helix, 1645 cm^{-1} unordered

Preprints (www.preprints.org) | NOT PEER-REVIEWED | Posted: 10 May 2022 doi:10.20944/preprints202205.0132.v1

structure and 1660, 1668, 1690 cm^{-1} turns and bends. Apart from an investigation of proteins in D_2O solutions, an analysis of thin dry films of Bovine Serum Albumin as a function of temperature was performed in ref. [30]. As our samples were dry CAB and also dried CAB@ferria, we adapted this approach taking advantage of the fact that IR-ATR can be used for spectra recording. We were not using the approach presented in ref. [31] of calculating the absorbance spectrum from recorded ATR using Kramers-Kronig transformation, but instead directly converted ATR reflectance into absorbance spectrum, which for the conclusions of this work appeared satisfying. The transformed ATR spectra of CAB, CAB@ferria, and ferria are presented in Fig. 3. It is possible to see that in the spectrum of ferria, apart from the bands around 570 cm^{-1}, characteristic for Fe_3O_4, bands due to absorbed water are also present[32].

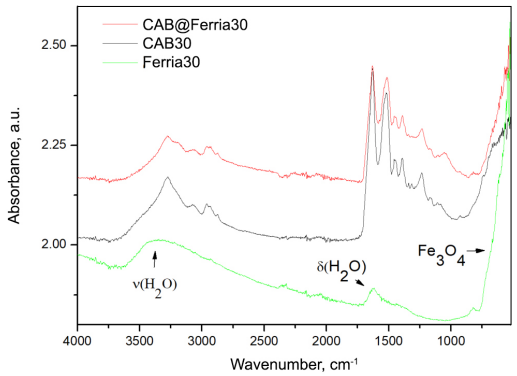

Figure 3. ATR converted to absorbance spectra of CAB@ferria, CAB and Ferria at 30 °C. The bands on ferria spectra are assigned are marked with arrows.

In order to be able to compare the native CAB spectra with the spectra of CAB which was caged in the Ferria cage, we subtracted the spectrum of ferria from the spectrum of CAB@Ferria at each temperature, respectively. Since the penetration depth of the radiation for different samples is different, which affects the absorbance band, a program was written in Mathematica program package that minimized the deviation between subtracted CAB@ferria and ferria spectra and the corresponding CAB spectrum. The spectra of CAB and the CAB@Ferria minus ferria spectra (in the further text C@F-F), at different temperatures, are presented in Fig. 4.

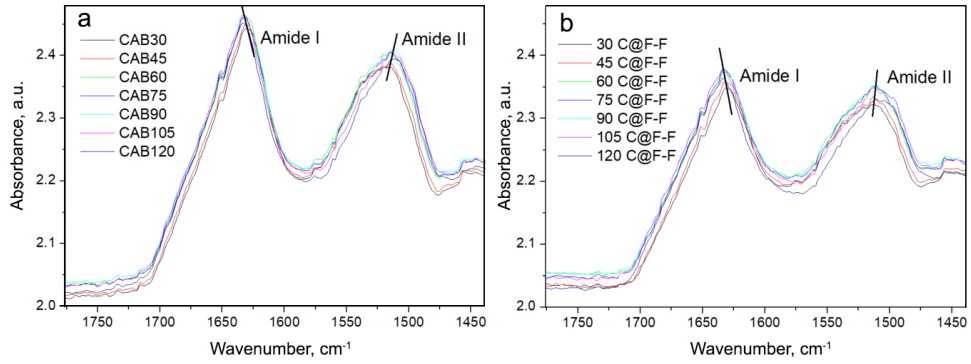

Figure 4. (**a**) ATR converted spectra of: Native CAB recorded at different temperature. (**b**) CAB spectra were obtained after subtraction of CAB@ferria and ferria spectra (named C@F-F), at different temperatures with a minimized difference. Amide I and Amide II frequency regions are presented. The lines indicate the tendency to shift the maxima of Amide I and Amide II bands with the temperature change.

One obvious feature in Fig. 4 is the shift of the Amide I band to higher frequencies and Amide II band to lower frequencies with the increase in temperature. This is due to the

Preprints (www.preprints.org) | NOT PEER-REVIEWED | Posted: 10 May 2022 doi:10.20944/preprints202205.0132.v1

weakening or breaking of hydrogen bonds in the protein[30]. Since Amide I band appears as a result of primarily ν(C=O) vibration, while Amide II is mostly due to ν(N-H), the above effect is obvious and appears in both CAB and C@F-F spectra. The range of the shift, in both cases, is about 2 cm^{-1}, for both Amide I and II bands. However, one difference between CAB and C@F-F spectra is that maximum of the Amide II band maximum at 30 °C for the former is located at 1513 cm^{-1}, while for the latter at 1510 cm^{-1}. Another difference is that at 120 °C, the Amide II shoulder is present at 1497 $^{-1}$ in the C@F-F spectrum, which is almost absent in the spectrum of CAB. What is also possible to see, is that apart from the shift of the maxima in Amide I and II bands, a change in the band profile with a change in temperature occurs. To see which of the bands that the Amide I and Amide II are composed of primarily changes with the temperature change, we subtracted the spectra of CAB at any temperature with the spectrum recorded at 120 °C. This was also done for the C@F-F spectra, where each spectrum was subtracted from the one at 120 °C. The difference spectra are presented in Fig. 5. Because the difference spectrum has a very low signal/noise ratio, we performed smoothing of the spectral lines.

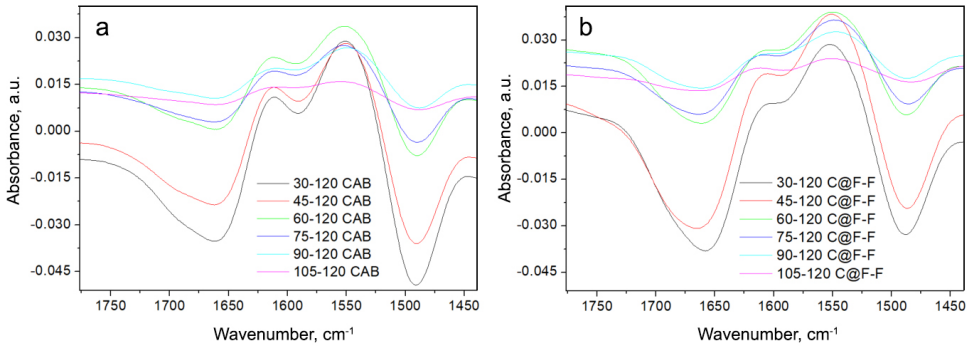

Figure 5. Difference spectra for CAB (**a**) and C@F-F (**b**), indicated through the label. Each spectrum is obtained as a difference between the spectrum obtained at a particular temperature and the one at 120 °C

From the change in the difference intensity of C@F-F spectra (Fig. 5a), it can be seen that the largest change occurs for the band minimum at 1657 – 1664 cm^{-1}, is in connection to the melting of the α-helix structure[27]. On the other hand, the change of the β-sheet is barely pronounced, checked through the difference band maximum (or better, shoulder) at 1601 – 1614 cm^{-1} (band position at the lowest temperature and the highest temperature). The changes in the difference spectra of CAB (Fig. 5b) are more or less the same, except that changes in the β-sheet are much more pronounced (the maximum at 1604 cm^{-1} is visible in any difference spectrum); another minima (appearing as a shoulder at 1700 cm^{-1}) is visibly present; the changes in the Amide I region are stronger than the one of Amide II, i.e. more C=O ... H hydrogen bonds are weakened or broken than N – H ... O, when compared to difference spectra of C@F-F.

Table 2. Minima and maxima in the difference spectra of CAB and C@F-F. The difference spectrum is between the spectrum at a particular temperature and the one recorded at 120 °C.

Position	min	min	max	min	max	min
μ(CAB)/cm^{-1}	1700	1661	1611	1591	1550	1490
μ(C@F-F)/cm^{-1}		1663	1604	1594	1551	1487

It is also possible to check the rate in the changes of the Amide I and II bands with the temperature if the difference between the spectra obtained at lower and the nearest higher temperature is calculated, as presented on Fig. 6.

Preprints (www.preprints.org) | NOT PEER-REVIEWED | Posted: 10 May 2022 doi:10.20944/preprints202205.0132.v1

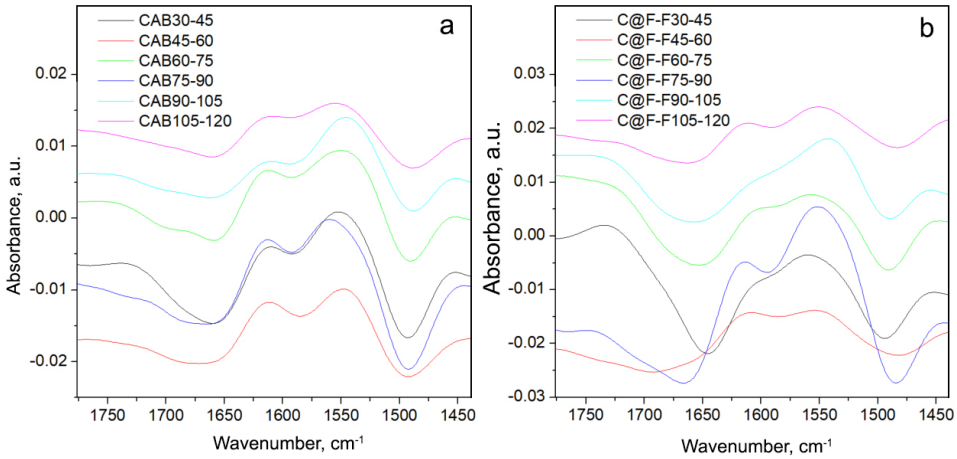

Figure 6. Difference spectra for CAB (**a**) and C@F-F (**b**). Each spectrum is obtained as difference between the spectrum obtained at lower and the nearest higher temperature.

It can be seen from Fig. 6 that the greatest change of the previously discussed band minima and maxima given in Fig. 5 and Table 2, occurs for the spectrum C@F-F75-90. This is not a coincidence, as at the temperature of 87 °C, the maximum in the cooperative melting of CAB was detected, for CAB in acidic D_2O solution[27]. Thus, the changes in the α- and β-structures will be the greatest for spectra recorded at temperatures before and after the maximum structural change. Particularly visible is the change of the β-structure, through the appearance of the max. at 1616 cm^{-1}, which is barely visible in the C@F-F30-45 and C@F-F45-60. On the other hand, there is a continuous change in the case of CAB. Thus, a similar effect may occur for CAB trapped in magnetite, i.e. a formation of a "molten-globule state". This is further supported by the irregular changes in the C@F-F30-45 and C@F-F45-60, as in the temperature range 10 – 67 °C a non-cooperative melting of the secondary structure might have occurred as reported for the case of acidic CAB[27]. Finally, it was also interesting to compare the differences between the CAB and the C@F-F spectra, with the temperature change. For that, the corresponding spectra at each temperature are subtracted from one another (Fig. 7).

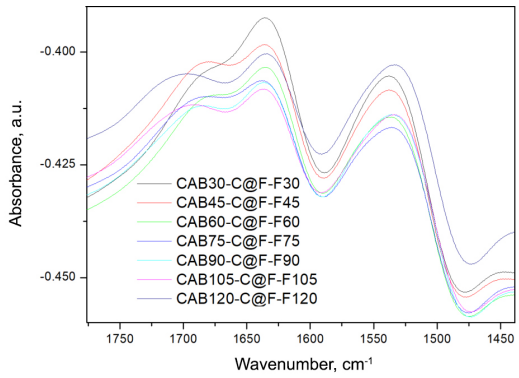

Figure 7. Difference spectra between CAB and C@F-F at each temperature

The difference spectra show several maxima and minima, which are connected to the relative presence of the secondary structure in CAB and CAB@Ferria. The maxima are connected to a greater relative presence in CAB, while the minima in the CAB@ferria. The maxima and minima are at frequencies: max 1679, 1638, 1535 cm^{-1}, min 1667, 1591, 1475 cm^{-1}. The band maxima at 1679 and 1638 cm^{-1}, coincide with the high and low component β-structure[28], while 1667 cm^{-1} with the α helical or unordered structure[27]. Thus, β-structures are more present in CAB, while α-helical or unordered structure in CAB@Ferria. Concerning relative changes in the intensities of these minima and maxima

Preprints (www.preprints.org) | NOT PEER-REVIEWED | Posted: 10 May 2022 doi:10.20944/preprints202205.0132.v1

and their frequency with temperature, it can be seen that they occur and that the most prominent changes are between spectra at 30 and 40 °C, and 105 and 120 °C. To investigate the stability of CAB and CAB@ferria samples, we increased the temperature to 90 °C (the temperature at which the activity may still be retained). The recorded spectra of these samples with the rise of the temperature are presented in Figs. 8 and 9.

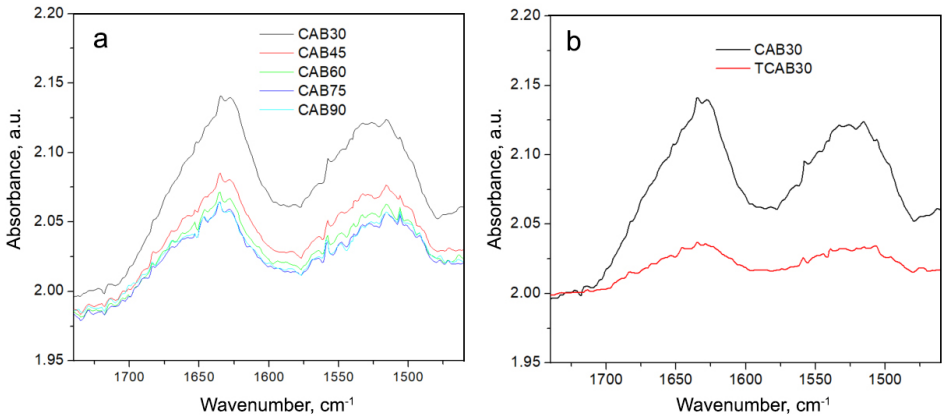

Figure 8. (**a**) Spectra of CAB recorded at different temperatures (from 30 to 90 °C with a step of 15 °C) in the region of Amide I and II vibrations. (**b**) Spectrum of CAB recorded at 30 °C (black curve); spectrum of CAB obtained at 30 °C after cooling from 90 °C (red curve).

From Fig. 8 it is easily seen that there is a change in band intensities and their form with temperature, but more important is that after cooling down to 30 °C, there is a big difference between that spectrum and the originally recorded CAB spectrum at 30 °C (Fig. 6b).

Again, the spectrum of CAB@Ferria changes with temperature as previously explained (Fig. 9a). However, when comparing the spectra of CAB@Ferria originally recorded at 30 °C (Fig. 9b, black curve) with the spectrum recorded at 30 °C after cooling from 90 °C, it is obvious that there is no difference between the bands either in intensity nor in the form. This means that the structure of the CAB@Ferria changes with temperature, and so does its activity, but after cooling the CAB@Ferria returns to its original structure, i.e. the process is reversible, which couldn't be said for CAB.

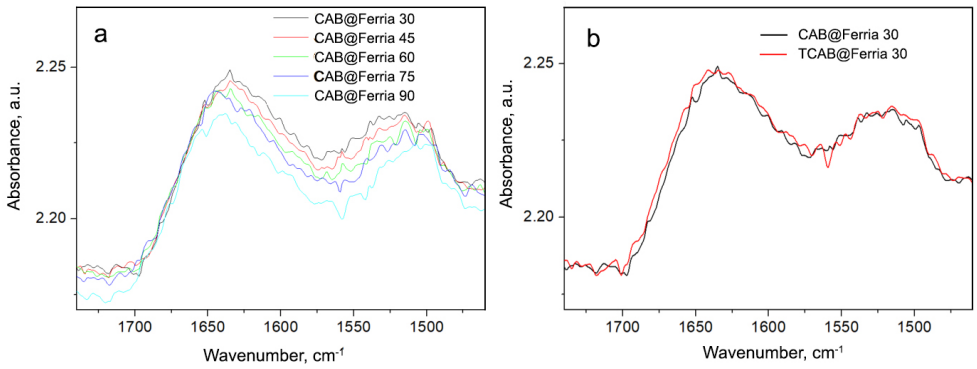

Figure 9. (**a**) Spectra of CAB@ferria recorded at different temperatures (from 30 to 90 °C with a step of 15 °C) in the region of Amide I and II vibrations. (**b**) Spectrum of CAB@ferri recorded at 30 °C (black curve); spectrum of CAB obtained at 30 °C after cooling from 90 °C (red curve)

3. Discussion

The problem of enzyme immobilization within sol-gel matrices is under intense investigation, and the list of the described systems is rising every day. The main attention

 doi:10.20944/preprints202205.0132.v1

is paid to silica-based biomaterials where new synthetic methodologies of entrapment are been developed, enzymatic activities are been analyzed and stability studies are been carried out[33]. The advantage of such materials was demonstrated in numerous studies, where silica solgel systems not only preserve the activity of the bioactive dopants but also provided exceptional chemical and thermal stability to a variety of proteins, enzymes, and even whole cells against various deterioration processes[34–37]. The attention towards silica materials is mainly dictated by their relative cheapness, convenience, and simple synthetic conditions, but alternative materials, such as alumina, titania, or iron oxide-based systems can also be used for this purposes[38–41]. In our work, we used the original approach toward entrapment of biomolecules within sol-gel magnetite matrix at mild conditions based on readily available water-based magnetite hydrosol. The hydrosol was synthesized without any surfactants to make it bio-friendly by design and prevent premature denaturation of biomolecules in the system and allow the system to undergo a sol-gel transition that would be prevented due to surface modification of the magnetite nanoparticles. Exceptional thermal stability of entrapped enzymes was demonstrated by many research groups and typically was associated with tight interaction of entrapped enzymes with the 3D structure of the sol-gel matrix within a single pore and surface-bound water molecules preserving the secondary structure of entrapped enzymes[17,42,43]. It is widely accepted that maintaining good hydration of the sol-gel matrix by mild synthetic conditions and in some cases, application of osmolytes play a key role in the stability of bio-doped ceramics even at high temperatures[44]. In the case of CAB@Ferria composite suitable hydration of the entrapped enzyme is maintained due to surface-bound water molecules whose IR bands can be observed even at 200 °C[45]. Since the structural integrity of biomolecules determines their bioactivity, this problem was investigated in a variety of way that describes the structural properties of biomolecules and their rearrangements in response to external stimuli[18,30,46,47]. Unfortunately, in the case of Ferria doped materials one of the most powerful techniques namely circular dichroism is unsuitable due to strong UV adsorption by magnetite nanoparticles, thus it was investigated via FTIR spectroscopy. IR-ATR investigations of CAB and CAB@ferria showed differences in their structural behavior with the temperature change. In both cases, there is a shift of the Amide I to higher and Amide II to lower frequencies with an increase in the temperature. The reason for this behavior is due to the weakening or breaking of hydrogen bonds in the protein. The maximum of the Amide II band in the CAB@ferria sample is at a lower wavenumber than in CAB, which might be in connection to some stronger hydrogen bonds. The difference spectra obtained when subtracting spectrum at a particular temperature with the one recorded at 120 °C, reveals that α-helix structures are more subjected to decomposition than β-structures in CAB than in CAB@ferria. The difference spectra obtained by subtraction of spectra recorded at neighboring temperatures reveal a possible "molten-globule state" in the CAB@Ferria sample. The difference spectra between CAB and CAB@ferria at each particular temperature, show that the ratio of α-helix structures (or unordered structures) to β-structures is greater in CAB@Ferria than in CAB. The structure of CAB@Ferria is reversible with temperature change, which couldn't be completely said for free CAB.

4. Conclusions

The two-component enzymatically active magnetic composite was synthesized via the sol-gel method using bio-friendly magnetite hydrosol at mild conditions by entrapment of CAB. The material showed exceptional thermal stability and was active at temperatures exceeding the denaturation temperature of the free enzyme for at least 20 °C. In this work, we made a first attempt to describe the observed stability of the entrapped enzyme by analyzing its secondary structure in response to thermal shock by using FTIR spectroscopy. The obtained results may be used as a basis for the development of bioactive magnetic ceramic materials with improved thermal stability.

 doi:10.20944/preprints202205.0132.v1

5. Materials and Methods

Chemicals: Carbonic anhydrase from bovine erythrocytes (CAB, cat. C-2624), Trisma hydrochloride, sodium hydroxide, iron (II) chloride tetrahydrate, iron (III) chloride hexahydrate, and ammonia were all obtained from Sigma-Aldrich. *Ferria hydrosol:* Ferria hydrosol was prepared by the procedure described earlier[5,48]. Briefly, 2.5 g of iron (II) chloride tetrahydrate and 5 g of iron (III) chloride hexahydrate were dissolved in 100 mL of deionized water and 11 mL of ammonia was added rapidly under constant stirring. The magnetic phase was magnetically separated and washed with water until a neutral pH level. After washing magnetic nanoparticles were dispersed in 100 mL of water and ultrasonically threatened for two hours. *Synthesis of CAB@Ferria:* The composite was produced by the procedure described in ref. [22] Briefly, 200 μL of Ferria was mixed with 20 μL of CAB solution 10 g/L in 0.05 M Tris buffer at pH 7.4 and dried under vacuum at 20 °C. The resulting composite was washed with Tris buffer and dried. *Enzymatic assay:* 1 mg of free CAB or equivalent mass of CAB@Ferria was dissolved in 2 mL of Tris buffer (pH 7.4) and incubated at a desired temperature for 10 minutes. After that, 125 μL of pNPA solution (0.8 M in acetone) was added, and enzymatic activity was spectrophotometrically measured at 405 nm in thermostatic conditions. As the control, the rate of pNPA self-hydrolysis alone and in the presence of empty Ferria sol-gel matrix was measures and subtracted from the experimental results. *IR-ATR spectroscopy:* The IR-ATR spectra were recorded on a Perkin-Elmer FT-IR System 2000 (USA) using Temperature controlled Golden Gate ATR accessory (product of Specac, UK), equipped with a diamond ATR crystal. The ZnSe lenses allowed ATR spectrum to be recorded as low as 520 cm-1. The spectra of the samples (CAB, CAB@Ferria, and Ferria) and the background (air/nitrogen) were recorded using 64 scans and 4 cm^{-1} resolution. Because the index of refraction of a medium depends on the temperature, the single-beam spectra were recorded at temperatures of 30, 45, 60, 75, 90, 105, and 120° in a row, for that background first, and then the sample spectra were recorded under the same conditions, without removing the sample. Around 10 min between the attained temperature and the corresponding measurement was allowed to pass, in order for the sample to obtain the correct temperature and changes in it due to the temperature occurred. The corresponding sample and background spectra (recorded at the same temperature) were afterward divided in order to obtain the ATR spectra of the samples. The sample compartment and detector were purged with nitrogen with 99.999% purity.

Author Contributions: "Conceptualization, A.D.; formal analysis, V.I. and A.D.; investigation, A.D., V.I. and O.S.; writing V.I and A.D.

Funding: This research was funded by the Russian Science Foundation, grant number 20-73-00001

Conflicts of Interest: The authors declare no conflict of interest

Abbreviations

The following abbreviations are used in this manuscript:

CAB	Carbonic anhydrase from bovine erythrocytes
NPs	nanparticles
DCS	dynamic scanning calorimetry
FTIR	Fourier-transform infrared spectroscopy
ATR	Attenuated total reflection pNPA
para-nitrophenylacetate	

References

References

1. Cipolatti, E.P.; Silva, M.J.A.; Klein, M.; Feddern, V.; Feltes, M.M.C.; Oliveira, J.V.; Ninow, J.L.; De Oliveira, D. Current status and trends in enzymatic nanoimmobilization. *Journal of Molecular Catalysis B: Enzymatic* **2014**, *99*, 56–67.
2. Kumar, A.; Sharma, S.; Pandey, L.M.; Chandra, P. Nanoengineered material based biosensing electrodes for enzymatic biofuel cells applications. *Materials Science for Energy Technologies* **2018**, *1*, 38–48.

3. Willner, I.; Basnar, B.; Willner, B. Nanoparticle–enzyme hybrid systems for nanobiotechnology. *The FEBS journal* **2007**, *274*, 302–309.
4. Sharifi, M.; Sohrabi, M.J.; Hosseinali, S.H.; Hasan, A.; Kani, P.H.; Talaei, A.J.; Karim, A.Y.; Nanakali, N.M.Q.; Salihi, A.; Aziz, F.M.; others. Enzyme immobilization onto the nanomaterials: application in enzyme stability and prodrug-activated cancer therapy. *International Journal of Biological Macromolecules* **2020**, *143*, 665–676.
5. Kolchanov, D.S.; Slabov, V.; Keller, K.; Sergeeva, E.; Zhukov, M.V.; Drozdov, A.S.; Vinogradov, A.V. Sol–gel magnetite inks for inkjet printing. *Journal of Materials Chemistry C* **2019**, *7*, 6426–6432.
6. Cottone, G.; Giuffrida, S.; Bettati, S.; Bruno, S.; Campanini, B.; Marchetti, M.; Abbruzzetti, S.; Viappiani, C.; Cupane, A.; Mozzarelli, A.; others. More than a confinement:"Soft" and "hard" enzyme entrapment modulates biological catalyst function. *Catalysts* **2019**, *9*, 1024.
7. Lei, Q.; Guo, J.; Noureddine, A.; Wang, A.; Wuttke, S.; Brinker, C.J.; Zhu, W. Sol–gel-based advanced porous silica materials for biomedical applications. *Advanced Functional Materials* **2020**, *30*, 1909539.
8. Gonçalves, M.C. Sol-gel silica nanoparticles in medicine: A natural choice. Design, synthesis and products. *Molecules* **2018**, *23*, 2021.
9. Avnir, D.; Braun, S.; Lev, O.; Ottolenghi, M. Enzymes and other proteins entrapped in sol-gel materials. *Chemistry of Materials* **1994**, *6*, 1605–1614.
10. Braun, S.; Rappoport, S.; Zusman, R.; Avnir, D.; Ottolenghi, M. Biochemically active sol-gel glasses: the trapping of enzymes. *Materials Letters* **1990**, *10*, 1–5.
11. Frenkel-Mullerad, H.; Ben-Knaz, R.; Avnir, D. Preserving the activity of enzymes under harsh oxidizing conditions: sol–gel entrapped alkaline phosphatase exposed to bromine. *Journal of sol-gel science and technology* **2014**, *69*, 453–456.
12. Pierre, A. The sol-gel encapsulation of enzymes. *Biocatalysis and Biotransformation* **2004**, *22*, 145–170.
13. Wang, J.; Monton, M.R.N.; Zhang, X.; Filipe, C.D.; Pelton, R.; Brennan, J.D. Hydrophobic sol–gel channel patterning strategies for paper-based microfluidics. *Lab on a Chip* **2014**, *14*, 691–695.
14. Ullah, S.; Seidel, K.; Türkkan, S.; Warwas, D.P.; Dubich, T.; Rohde, M.; Hauser, H.; Behrens, P.; Kirschning, A.; Köster, M.; others. Macrophage entrapped silica coated superparamagnetic iron oxide particles for controlled drug release in a 3D cancer model. *Journal of Controlled Release* **2019**, *294*, 327–336.
15. Imam, H.T.; Marr, P.C.; Marr, A.C. Enzyme entrapment, biocatalyst immobilization without covalent attachment. *Green Chemistry* **2021**, *23*, 4980–5005.
16. Luckarift, H.R.; Spain, J.C.; Naik, R.R.; Stone, M.O. Enzyme immobilization in a biomimetic silica support. *Nature biotechnology* **2004**, *22*, 211–213.
17. Brennan, J.D.; Benjamin, D.; DiBattista, E.; Gulcev, M.D. Using sugar and amino acid additives to stabilize enzymes within sol- gel derived silica. *Chemistry of materials* **2003**, *15*, 737–745.
18. Vinogradov, V.V.; Avnir, D. Exceptional thermal stability of therapeutical enzymes entrapped in alumina sol–gel matrices. *Journal of Materials Chemistry B* **2014**, *2*, 2868–2873.
19. Yi, Y.; Chen, Y.; Brook, M.A.; Brennan, J.D. Development of macroporous titania monoliths by a biocompatible method. Part 2: Enzyme entrapment studies. *Chemistry of materials* **2006**, *18*, 5336–5342.
20. Shi, X.; Gu, W.; Li, B.; Chen, N.; Zhao, K.; Xian, Y. Enzymatic biosensors based on the use of metal oxide nanoparticles. *Microchimica Acta* **2014**, *181*, 1–22.
21. Shabanova, E.M.; Drozdov, A.S.; Ivanovski, V.; Suvorova, I.I.; Vinogradov, V.V. Collagenase@ magnetite: proteolytic composite for magnetically targeted minimally invasive surgery. *RSC advances* **2016**, *6*, 84354–84362.
22. Drozdov, A.S.; Shapovalova, O.E.; Ivanovski, V.; Avnir, D.; Vinogradov, V.V. Entrapment of enzymes within sol–gel-derived magnetite. *Chemistry of Materials* **2016**, *28*, 2248–2253.
23. Andreeva, Y.I.; Drozdov, A.S.; Avnir, D.; Vinogradov, V.V. Enzymatic nanocomposites with radio frequency field-modulated activity. *ACS Biomaterials Science & Engineering* **2018**, *4*, 3962–3967.
24. Anastasova, E.I.; Ivanovski, V.; Fakhardo, A.F.; Lepeshkin, A.I.; Omar, S.; Drozdov, A.S.; Vinogradov, V.V. A pure magnetite hydrogel: synthesis, properties and possible applications. *Soft matter* **2017**, *13*, 8651–8660.
25. Tilton Jr, R.F.; Dewan, J.C.; Petsko, G.A. Effects of temperature on protein structure and dynamics: X-ray crystallographic studies of the protein ribonuclease-A at nine different temperatures from 98 to 320K. *Biochemistry* **1992**, *31*, 2469–2481.
26. QI, X.L.; HOLT, C.; MCNULTY, D.; CLARKE, D.T.; BROWNLOW, S.; JONES, G.R. Effect of temperature on the secondary structure of β-lactoglobulin at pH 6.7, as determined by CD and IR spectroscopy: a test of the molten globule hypothesis. *Biochemical Journal* **1997**, *324*, 341–346.
27. Brazhnikov, E.; Chirgadze, Y.N.; Dolgikh, D.; Ptitsyn, O. Noncooperative temperature melting of a globular protein without specific tertiary structure: Acid form of bovine carbonic anhydrase B. *Biopolymers: Original Research on Biomolecules* **1985**, *24*, 1899–1907.
28. Byler, D.M.; Susi, H. Examination of the secondary structure of proteins by deconvolved FTIR spectra. *Biopolymers: Original Research on Biomolecules* **1986**, *25*, 469–487.
29. Montich, G.G. Partly folded states of bovine carbonic anhydrase interact with zwitterionic and anionic lipid membranes. *Biochimica et Biophysica Acta (BBA)-Biomembranes* **2000**, *1468*, 115–126.

30. Grdadolnik, J.; Maréchal, Y. Bovine serum albumin observed by infrared spectrometry. I. Methodology, structural investigation, and water uptake. *Biopolymers: Original Research on Biomolecules* **2001**, *62*, 40–53.
31. Grobelnik, B.; Grdadolnik, J. Calculation of the Absorption Spectrum from an ATR Infrared Experiment. *Acta Chimica Slovenica* **2008**, *55*.
32. Li, Y.S.; Church, J.S.; Woodhead, A.L. Infrared and Raman spectroscopic studies on iron oxide magnetic nano-particles and their surface modifications. *Journal of Magnetism and Magnetic Materials* **2012**, *324*, 1543–1550.
33. Avnir, D.; Coradin, T.; Lev, O.; Livage, J. Recent bio-applications of sol–gel materials. *Journal of Materials Chemistry* **2006**, *16*, 1013–1030.
34. Jafari, H.; Amiri, M.; Abdi, E.; Navid, S.L.; Bouckaert, J.; Jijie, R.; Boukherroub, R.; Szunerits, S. Entrapment of uropathogenic E. coli cells into ultra-thin sol-gel matrices on gold thin films: A low cost alternative for impedimetric bacteria sensing. *Biosensors and Bioelectronics* **2019**, *124*, 161–166.
35. Ganonyan, N.; Benmelech, N.; Bar, G.; Gvishi, R.; Avnir, D. Entrapment of enzymes in silica aerogels. *Materials Today* **2020**, *33*, 24–35.
36. Fernandez Caresani, J.R.; Dallegrave, A.; dos Santos, J.H. Amylases immobilization by sol–gel entrapment: Application for starch hydrolysis. *Journal of Sol-Gel Science and Technology* **2020**, *94*, 229–240.
37. Pylypchuk, I.V.; Daniel, G.; Kessler, V.G.; Seisenbaeva, G.A. Removal of diclofenac, paracetamol, and carbamazepine from model aqueous solutions by magnetic sol–gel encapsulated horseradish peroxidase and lignin peroxidase composites. *Nanomaterials* **2020**, *10*, 282.
38. Drozdov, A.S.; Fakhardo, A.F.; Vinogradov, V.V. Sol-gel composites based on alumina and ferria for cardiovascular diseases treatment. In *Biocompatible Hybrid Oxide Nanoparticles for Human Health*; Elsevier, 2019; pp. 149–179.
39. Shapovalova, O.E.; Levy, D.; Avnir, D.; Vinogradov, V.V. Protection of enzymes from photodegradation by entrapment within alumina. *Colloids and Surfaces B: Biointerfaces* **2016**, *146*, 731–736.
40. Yu, J.; Ju, H. Preparation of porous titania sol- gel matrix for immobilization of horseradish peroxidase by a vapor deposition method. *Analytical chemistry* **2002**, *74*, 3579–3583.
41. Kochana, J.; Gala, A.; Parczewski, A.; Adamski, J. Titania sol–gel-derived tyrosinase-based amperometric biosensor for determination of phenolic compounds in water samples. Examination of interference effects. *Analytical and bioanalytical chemistry* **2008**, *391*, 1275–1281.
42. Eggers, D.K.; Valentine, J.S. Crowding and hydration effects on protein conformation: a study with sol-gel encapsulated proteins. *Journal of molecular biology* **2001**, *314*, 911–922.
43. Lin, S.; Van den Bergh, W.; Baker, S.; Jones, J.R. Protein interactions with nanoporous sol–gel derived bioactive glasses. *Acta Biomaterialia* **2011**, *7*, 3606–3615.
44. Nguyen, D.T.; Smit, M.; Dunn, B.; Zink, J.I. Stabilization of creatine kinase encapsulated in silicate sol- gel materials and unusual temperature effects on its activity. *Chemistry of Materials* **2002**, *14*, 4300–4306.
45. Drozdov, A.S.; Ivanovski, V.; Avnir, D.; Vinogradov, V.V. A universal magnetic ferrofluid: Nanomagnetite stable hydrosol with no added dispersants and at neutral pH. *Journal of colloid and interface science* **2016**, *468*, 307–312.
46. Portaccio, M.; Della Ventura, B.; Mita, D.; Manolova, N.; Stoilova, O.; Rashkov, I.; Lepore, M. FT-IR microscopy characterization of sol–gel layers prior and after glucose oxidase immobilization for biosensing applications. *Journal of sol-gel science and technology* **2011**, *57*, 204–211.
47. Delfino, I.; Portaccio, M.; Della Ventura, B.; Mita, D.; Lepore, M. Enzyme distribution and secondary structure of sol–gel immobilized glucose oxidase by micro-attenuated total reflection FT-IR spectroscopy. *Materials Science and Engineering: C* **2013**, *33*, 304–310.
48. Rumyantceva, V.; Rumyantceva, V.; Andreeva, Y.; Tsvetikova, S.; Radaev, A.; Vishnevskaya, M.; Vinogradov, V.; Drozdov, A.S.; Koshel, E. Magnetically controlled carbonate nanocomposite with ciprofloxacin for biofilm eradication. *International journal of molecular sciences* **2021**, *22*, 6187.